Research Article

NMR IN BIOMEDICINE

Received: 26 June 2008, Accepted: 12 November 2008, Published online in Wiley InterScience: 2 January 2009

(www.interscience.wiley.com) DOI:10.1002/nbm.1359

Trading off SNR and resolution in MR images

Shoan C. Kale [a,b], X. Josette Chen [a,b]* and R. Mark Henkelman [a,b]

With a fixed time to acquire a magnetic resonance (MR) image, time can be spent to acquire better spatial resolution with decrease in signal-to-noise ratio (SNR) or decreased resolution with increase in SNR. This resolution/SNR tradeoff at fixed time has been investigated by a visual rater study using images of *ex vivo* mouse brains. Simulated images with a tradeoff between SNR and resolution were produced from high-quality, 3D isotropic mouse brain images to emulate shorter constant acquisition times. The tradeoff images spanned a range of SNRs (63–6) and isotropic resolutions (32–81 μm). Fourteen readers identified the image which best displayed neuroanatomy. Additional experiments tested for (i) intra-observer consistency, (ii) the effect of emulated scan time, and (iii) specifically biased questions pertaining to the perception of neuroanatomy. Optimal anatomical viewing depended primarily on the SNR of the images. Specifically, for fixed imaging time, preference lay in the SNR range of ∼30–35 with strong consistency and there was minimal effect from overall imaging time. Copyright © 2009 John Wiley & Sons, Ltd.

Keywords: MRI; signal-to-noise ratio; fixed imaging time; tradeoff; resolution

INTRODUCTION

Magnetic resonance (MR) imaging gives exceptional anatomical images on account of the excellent soft tissue contrast. The user has appreciable flexibility over the appearance of the resulting images with regard to the field-of-view, contrast, resolution, orientation, and isotropy of data.

One of the main appreciable limitations in MR imaging is the inherently noisy data. The dominant sources of noise in an MR image originate from thermal fluctuations of electrolytes in the subject and electrons in the receiver coil (1–3). To improve image quality through increased signal-to-noise ratio (SNR), technological advances have been made in receiver coil geometry, parallel imaging using multiple coils (4), gradient engineering and pulse sequence design (5), high temperature superconducting receiver coils (6), and sophisticated image post-processing techniques. In spite of these efforts, imaging time remains a key limiting factor to improving image quality.

Normally, increasing the scan time in MR imaging offers improved image quality, which can be expended for increasing the resolution, SNR, or both. Image resolution can be increased (i.e. voxel volume decreased) by spending additional scan time to acquire higher frequency data in *k*-space. Alternatively, scan time can be spent on signal averaging, thus reducing the image noise and improving voxel SNR. However, no matter what the prescribed scan time is, a decision has to be made as to the tradeoff between SNR and resolution for the final image. Note that this SNR–resolution decision in MR imaging is irrevocable, unlike the situation with ionizing radiation modalities where the tradeoff choice is recoverable (7–9). For an excellent review of this comparison, see Edelstein *et al.* (8). Thus, to optimize images in MRI, it is important to select acquisition parameters with an ideal balance between SNR and resolution.

In this paper, we investigate the SNR–resolution tradeoff that provides optimal visualization of neuroantomy. Images taken at a constant time but with differing tradeoffs between SNR and resolution were simulated from extremely high-quality images of mouse brains. Additional experiments were performed to assess (i) the inter- and intra-reader variability; (ii) the effect of the prescribed time available for data acquisition and (iii) the effect on the perception of neuroanatomy given differing evaluation criteria. The purpose of this work is to provide guidance on the optimal choice of tradeoff between SNR and resolution to make the most effective use of scan time.

MATERIALS AND METHODS

We conducted this study using images of fixed mouse neuroanatomy acquired through a high-quality microscopy protocol developed at the Mouse Imaging Centre (Toronto, Canada). Brain specimens were imaged in the skull to preserve the natural conformation of the brain and were prepared by methods described previously (10,11). All animal protocols were approved by the Hospital for Sick Children.

* *Correspondence to: X. J. Chen, Mouse Imaging Centre, Hospital for Sick Children, Toronto Centre for Phenogenomics, 25 Orde Street, Toronto, Ontario M5T 3H7, Canada.*
E-mail: josette@phenogenomics.ca

a *S. C. Kale, X. J. Chen, R. M. Henkelman*
Mouse Imaging Centre, Hospital for Sick Children, Toronto, Ontario, Canada

b *S. C. Kale, X. J. Chen, R. M. Henkelman*
Department of Medical Biophysics, University of Toronto, Toronto, Ontario, Canada

Contract/grant sponsor: Canada Foundation for Innovation and the Ontario Innovation Trust (funds for infrastructure for the Mouse Imaging Centre), Burroughs Wellcome Fund, the Canadian Institutes of Health Research, the National Cancer Institute of Canada, the National Institutes of Health Research and the Ontario Consortium for Small Animal Imaging.

Abbreviations used: *SNR, signal-to-noise ratio; MR, magnetic resonance; NSERC, Natural Sciences and Engineering Research Council; PBS, phosphate buffered saline; PFA, paraformaldehyde; FSE, Fast spin-echo; TR, repetition time; TE, time to echo; $TE_{effective}$, time to echo corresponding to the center of k-space; RAM, random access memory; NA, number of averages; ROI, region of interest; $\overline{SNR_w}$, weighted mean signal-to-noise ratio; MICe, mouse imaging center; PE, phase encode; RO, read out.*

Copyright © 2009 John Wiley & Sons, Ltd.

Preparation

Ten genetically identical male and female C57BL/6J wildtype mice (~6 weeks of age) were anesthetized using a mixture of Rompun (Bayer Animal Health, Toronto, ON) (20 mg/kg) and Ketamine (Pfizer Animal Health, Kirkland, QC) (100 mg/kg). The animals were perfused with 30-mL phosphate-buffered saline (PBS) allowing the drainage of blood and then fixed with 30-mL of iced 4% paraformaldehyde (PFA) prior to decapitation. The skin, lower jaw, ears, nose tip, and zygomatic bones were removed from the heads. The remaining skull–brain structures were placed in a bath of 4% PFA for 4–5 h at 4°C, and then nutated in a solution containing PBS and 0.01% sodium azide for seven days to wash out the PFA followed by seven days in a solution including a 2 mM concentration of contrast agent Prohance® (Bracco Diagnostics Canada, Mississauga, ON). Imaging of specimens was performed within 5–6 months following this preparation, during which time the brains were refrigerated in the contrast agent at 4°C. Prior to imaging, brains were blotted and immersed in Fluorinert™ (3M Specialty Materials, St. Paul, MN) within a plastic tube to provide susceptibility matching without signal from the immersion fluid.

Imaging

Imaging was performed on a 7-T superconducting magnet (Magnex Scientific, Oxford, UK) connected to a multichannel Varian^{INOVA} console (Varian NMR Instruments, Palo Alto, CA). The mean values of T_1 and T_2 in the brain were measured to be 175 ± 16 and 28 ± 2 ms, respectively. A six-echo fast spin-echo (FSE) pulse sequence was used (TR/echo train spacing = 325/8 ms) with the center of *k*-space acquired on the fourth echo ($TE_{effective} = 32$ ms), a 90° flip angle, a $14 \times 14 \times 25$ mm^3 FOV, an acquisition matrix of $432 \times 432 \times 780$, and four averages (NA). Using parallel acquisitions and independent solenoid coils, three brains were imaged concurrently (10) in a total scan time of 11.3 h. The protocol yielded T_2-weighted images with 32-μm isotropic resolution. Images were reconstructed on a 2-GHz dual-processor, 64-bit Linux workstation with 8-GB RAM, using Matlab R13 (MathWorks, Natick, MA). The mean SNR in homogeneous gray matter was 16 across the 10 scanned brains.

Data simulation

The acquired data of high quality (henceforth referred to as reference data) were degraded to simulate shorter, constant acquisition times, but at the expense of SNR and resolution. Data were simulated for acquisition times of 1.8 h. The procedure described below was applied to each of the ten reference brains. We used simulated data to avoid confounds from specimen degradation or scanner instability.

In the first step, resolution was degraded starting with one full *k*-space data-set and then sequentially retaining smaller central volumes corresponding to image voxel volumes that increased in size by $2\times$ at each step (equivalently, $\sqrt[3]{2}\times$ in each dimension). These volumes were designated as *A*, *B*, *C*, *D*, and *E* (Table 1). Given that both phase-encode dimensions of tradeoffs *B*–*E* decreased, the effective imaging time among tradeoffs also decreased to the point where *E* represented the lowest imaging time of 1.8 h. In the second step, the effective imaging time for all volumes was reduced to 1.8 h. At 1.8 h image *E* comprises four averages. The number of averages NA achievable in the same 1.8 h degrades for images *D* to *A* by the number of phase encodes (fifth column of Table 1). Decreased NA was simulated by adding zero mean, Gaussian white noise to the *k*-space tradeoff volumes *A*–*D* (12). Since variances add, the specific amount of noise added to the real and imaginary channels of *k*-space for each tradeoff *i* was $\sqrt{\sigma_{tar}^{i}2 - \sigma_k^2}$. Here, σ_{tar} is the target standard deviation of noise which emulates the reduced signal averaging for tradeoff *i* and σ_k is the standard deviation of noise in the *k*-space data prior to noise addition. The standard deviation of noise in *k*-space, σ_k, was measured from the mean of the standard deviations of noise in a signal- and artifact-free region of complex image space of the reference image prior to noise addition (12). Random simulated noise was generated using the normal-distribution random number generator in Matlab, which samples from the entire normal distribution with a period much greater than the number of samples generated. Finally, tradeoff image sets were produced by this procedure for each of the reference images acquired from the ten mice. The mean SNR of tradeoff groups *A*–*E* is reported in Table 1 for a homogeneous gray matter region of the brain. Note that the relationship linking SNR to sampling parameters and voxel size, given by Nishimura (3), $SNR \propto \Delta x \Delta y \Delta z \sqrt{\Delta t_{sampling}} \sqrt{NA}$, where $(\Delta x \Delta y \Delta z)$ is the change in voxel volume and $\Delta t_{sampling}$ is the change in total sampling time in a single experiment, corresponds to the simulated mean SNR values within 1%.

In an additional experiment, three more tradeoff images, *F*–*H*, were simulated from each of the reference data for a longer effective imaging time of 4.5 h. Details of this data are found in Table 2. Note that in this implementation of simulating

Table 1. Simulated 1.8-h tradeoff images[a]

Tradeoff	Voxel volume (mm × 10)^3	*k*-Space samples ($PE_1 \times PE_2 \times RO$)	Isotropic resolution[b] (μm)	Relative NA[c]	Mean SNR[d]
A	0.033	$432 \times 432 \times 780$	32	0.63	6.4
B	0.066	$344 \times 344 \times 620$	40	1.0	11.3
C	0.131	$272 \times 272 \times 492$	51	1.6	20.2
D	0.262	$216 \times 216 \times 390$	64	2.5	35.9
E	0.524	$172 \times 172 \times 310$	81	4.0	63.0

[a]Specifications for the first set of images simulated from the reference data by trading up resolution, signal averaging (SNR) or both for a fixed effective imaging time of 1.8 h.
[b]The isotropic resolution step between tradeoff images is $\sqrt[3]{2} \approx 1.26$.
[c]The relative NA between tradeoffs is $\left(\sqrt[3]{2}\right)^2 \approx 1.59$.
[d]The SNR step between tradeoffs is $\left(\sqrt[3]{2}\right)^{5/2} \approx 1.78$.

Copyright © 2009 John Wiley & Sons, Ltd.

Table 2. Simulated 4.5-h tradeoff images[a]

Tradeoff	Voxel volume (mm × 10)^3	*k*-space samples ($PE_1 \times PE_2 \times RO$)	Isotropic resolution (μm)	Relative NA	Mean SNR
F	0.033	432 × 432 × 780	32	1.6	10.0
G	0.066	344 × 344 × 620	40	2.5	18.3
H	0.131	272 × 272 × 492	51	4.0	32.9

[a]Specifications of the resolutions and SNRs for the second set of images generated for an effective imaging time of 4.5 h, the geometric mid-point between the acquisition times of the reference and 1.8-h tradeoff data.

SNR–resolution tradeoff images, it was assumed that TR was long enough such that the readout acquisition was never time limited, allowing for a constant bandwidth. As readout time increased, apodization from T_2 was ignored.

As brains were not fixed into a stereotactic coordinate system in the imaging procedure, small positional variations were observable amongst the imaged reference brains. To preserve left–right symmetry for viewing anatomy, comparative oblique slices were selected from the images.

Reader evaluation

To evaluate the SNR–resolution tradeoff, 14 readers were chosen who were graduate students and staff in the laboratory and well acquainted with viewing medical images. Corresponding horizontal slices from tradeoff images *A–E* of a given brain, chosen near the center of the brain, were concurrently displayed on a 19 in flat panel monitor (1280 × 1024 native resolution) in ambient lighting conditions. To avoid any possible bias in image evaluation resulting from the order of displayed images, the tradeoff images were randomly ordered in each presentation and shown in one row. Given the discretion over window/level, zoom, and pan (which were synchronized across all tradeoff images), readers were requested to make first and second choices in response to the question "Which image shows neuroanatomy best?" Readers had to evaluate contrasts and structures at varying scales among the tradeoff images. Readers were allowed as much time as they required to make an informed decision. The first and second choice tradeoff images were assigned weighted scores of 1 and 0.5. This task was repeated for each of the ten sets of tradeoff images.

This basic experiment (referred to as experiment 1) was then repeated four more times with modifications to test further issues. The additional experiments, numbered 2–5, were as follows:

Experiment 2: Coronal slices were used on a subsequent occasion 1–7 days later to test for reader consistency and independence of view orientation.

Experiment 3: The task was switched to focus on subtle changes in contrast by changing the question to "In which image can you best distinguish subtle contrast differences between brain regions?"

Experiment 4: The task was switched to focus on fine detail by changing the question to "In which image can you best visualize fine structure and details in the brain?"

Experiment 5: The three tradeoff images *F–H*, corresponding to a longer imaging time of 4.5 h, were used to evaluate the effect of overall image time and hence quality.

Experiments 3 and 4 requested only a first choice response (assigned a score of 1). There were no specific time delays for experiments 3–5.

Mean scores were computed over 140 repeats (10 brains × 14 readers) for all experiments. Reported errors about mean values, and associated error bars, represent the standard error of the mean normalized over the 140 repeats.

RESULTS

Data acquisition and simulation

Horizontal and coronal images from one brain volume of the acquired reference data are shown in the leftmost panels of Fig. 1. The slices selected correspond to the slices from the tradeoff data viewed by readers. Magnified regions-of-interest (ROIs) from the tradeoff images simulated for the corresponding brain at the 1.8- and 4.5-h effective imaging times are shown to the right of the reference slices (see figure caption). These ROIs were not specifically shown to the readers. High contrast details from the folia of the cerebellum and a subtle contrast change between the striatum and cortex are featured in ROIs 1 and 2. The arrowheads were not present in the viewer images. Images with the highest resolution (*A* and *F*) also have the maximum noise. At the other extreme, tradeoffs *E* and *H* have the highest SNRs, but are compromised by decreased spatial resolution. The contrast and resolution of the reference images are appreciable when compared to these tradeoff images. The range of image quality seen in these example tradeoff images is representative of all ten brains.

Reader evaluation

The time spent in examining images varied widely among the 14 readers and the four experiments. The median reading times for all ten mice were 14.5 min for experiment 1, 11.0 min for experiment 2, 6.2 min for experiments 3 and 4, and 8.5 min for experiment 5.

Results of experiment 1 are plotted in Fig. 2 as the mean score over the first and second choice preferences for each tradeoff group. The scores are broken down into first and second choices. One can see that tradeoff *D* is preferred when considering only first choices or both first and second choices. Note that the error bar for the score of tradeoff *D* does not overlap the errors of the

Copyright © 2009 John Wiley & Sons, Ltd.

NMR IN BIOMEDICINE

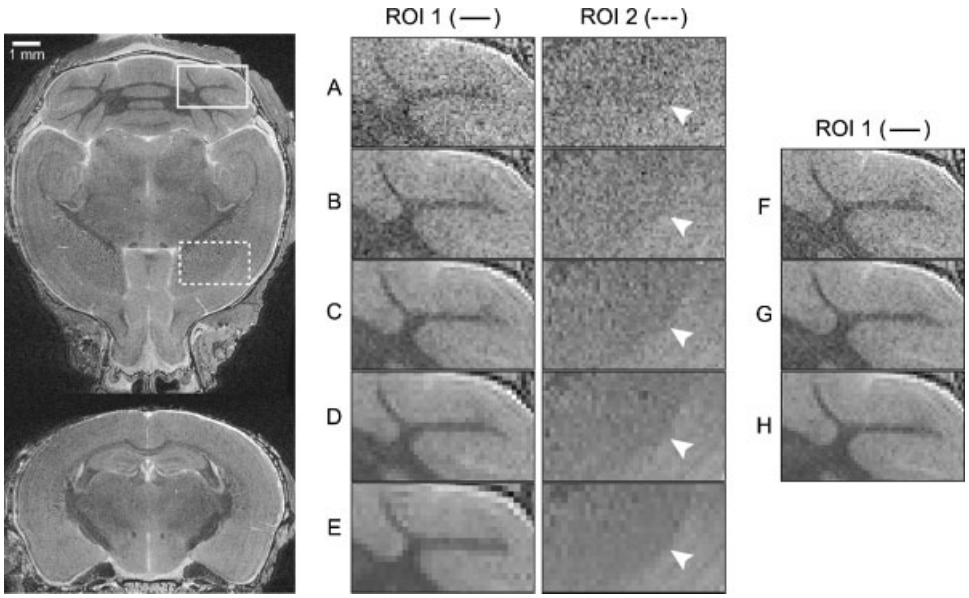

Figure 1. Isotropic imaging results from the high-resolution, high SNR imaging protocol with magnified ROIs from the tradeoff images. The far left images are orthogonal slices from one brain of the reference data with high resolution and SNR. The two outlined rectangles correspond to ROIs 1 (solid) and 2 (dashed) where the tradeoff images are sampled in the panels to the right. The two central columns of panels show the amounts of partial volume averaging and contrast across tradeoff images *A–E* in regions of the brain with high contrast details in the folia of the cerebellum (ROI 1, left of center), and a subtle contrast change between the striatum and the cortex (ROI 2, right of center). The arrowheads indicate the boundary between the striatum and the cortex (not included in the viewer images). The column of panels on the far right is the corresponding ROI 1 images for the 4.5-h tradeoff data, labeled *F–H*. ROIs are magnified by ~2.6×.

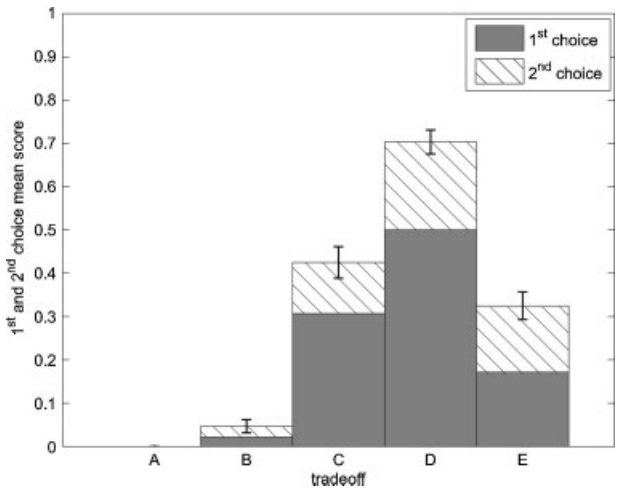

Figure 2. Reader scores of tradeoff images *A–E* in experiment 1 broken down by first choice (shaded) and second choice (diagonal pattern) mean scores. The mean scores and the error bars (representing the standard error of the mean) are normalized by the number of readers and the number of mice. Tradeoff *D*, with SNR~36, is most preferred when considering either the first choice scores alone or the combined score (both choices).

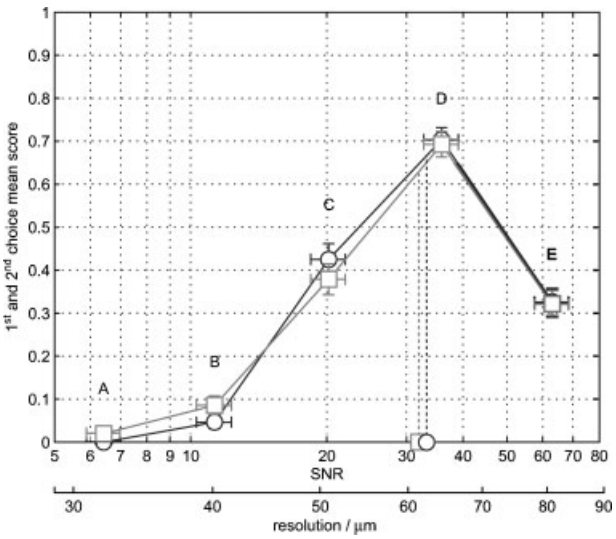

Figure 3. First and second choice mean scores *versus* mean SNR for horizontal (○) and coronal (□, retest) images, corresponding to experiments 1 and 2. The optimal image is evident at tradeoff *D* in both experiments with nearly identical scoring. The nearly overlapping vertical dashed lines represent the score-weighted geometric means of the two experiments. The equivalent isotropic resolution scale is appended below the plot. The horizontal error bars represent standard error of the mean.

other tradeoffs suggesting both consistency over all mice and strong significance for this tradeoff. The overall mean scores, which are composed of first and second selections, are similarly presented in succeeding figures without this explicit decomposition.

Scores for experiment 1 and 2 (retest) are shown plotted as a function of SNR in Fig. 3. Preference lies strongly for tradeoff *D*, with mean SNR of approximately 36, in both test and retest experiments with nearly identical scoring in each case. The intra-reader consistency, or the number of times a reader's first choice was the identical image in the retest experiment, was 56%, which is moderate. However, this value increases dramatically to 98% when determining the proportion of times a reader chose either their first or second choice, with order ignored, suggesting

 Copyright © 2009 John Wiley & Sons, Ltd.

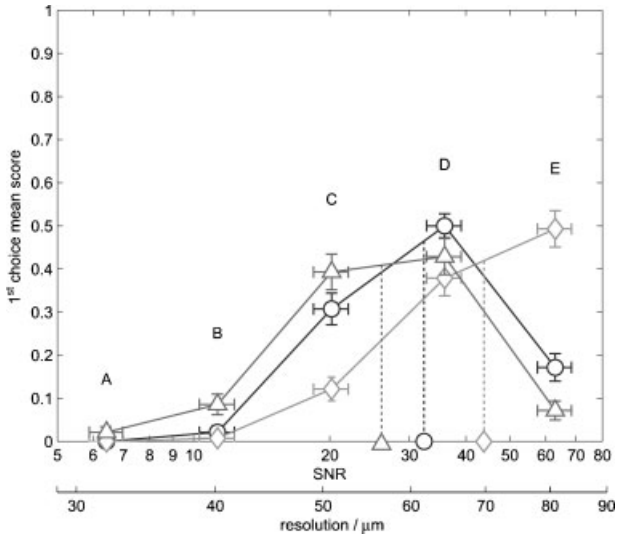

Figure 4. First choice mean score *versus* mean SNR for experiment 1 (○, determining best neuroanatomy), and experiment 3 (◇, distinguishing subtle contrast) and experiment 4 (Δ, visualizing fine structure). Note that the mean scores for the first choice preferences for experiment 1 (shaded bars, Fig. 2) are plotted instead of the composition of first and second choice presented in Fig. 3. The dashed lines descending from each curve represent the weighted mean preferred SNRs ($\overline{SNR_w}$). $\overline{SNR_w}$ lies at 32 for experiment 1. The $\overline{SNR_w}$ values are shifted higher to 44 for experiment 3 and lower to 26 for experiment 4.

that readers were strongly committed to only two of the tradeoff images. The consistency of the test and retest experiments also implies that reader choices were independent of the viewing axis, as hypothesized. The weighted mean preferred SNRs ($\overline{SNR_w}$), computed as the score-weighted geometric means (13), were 33.2 and 32.0 for the test and retest experiments (a percentage difference of less than 4%).

Figure 4 shows the results of the experiments when the task posed to readers was more specifically biased (experiments 3 and 4). The first choice mean scores from experiment 1 (shaded bars in Fig. 2) are also plotted for comparison. Based on the calculated values of $\overline{SNR_w}$ relative to experiment 1, we see that experiment 3 (reader focused on diffuse contrast) caused readers to choose tradeoff images with higher SNR and lower resolution. In contrast, experiment 4 (reader focused on high contrast detail) showed a shift of chosen optimum toward images with higher resolution and lower SNR. This indicates that highly specific viewing tasks require somewhat different tradeoff SNRs. This experiment also implies that readers balanced the conflicting objectives in experiments 3 and 4 when making their decisions in experiment 1. This is important in that it shows that readers were not choosing based on either SNR or resolution alone. While it is apparent that the tradeoff images are terminated prematurely at high SNR, particularly for experiment 3, enough of the plots are available to show the trends and make reasonable estimates of the weighted mean optimal SNRs, although the $\overline{SNR_w}$ for experiment 3 may be underestimated.

The purpose of experiment 5 was to investigate the effect of overall image quality on preference by having readers evaluate the data simulated for the 4.5-h imaging time. Scores for this data are plotted in Fig. 5, with results from experiment 1 also plotted for comparison. Scores are plotted against both SNR and resolution. The dashed lines represent the weighted mean preferred SNRs and resolutions for the plots on the left and right, respectively. Immediately apparent is that tradeoff *H*, with mean SNR 33, was optimal among the 4.5-h data. The proximity of $\overline{SNR_w}$ values in experiments 1 and 5 implies that readers' choices of optimal tradeoff images is determined primarily by SNR, whereas the obvious separation of the weighted mean optimal resolutions of these same data confirm that resolution is not the determining factor.

The 4.5-h simulation time-point was initially chosen as it is the geometric midpoint between the imaging time of the reference data (11.3 h) and the 1.8-h tradeoff data, and provided acceptable tradeoff images that were visually different (improved) from the 1.8-h tradeoff data. However, we were limited in SNR for the tradeoff images generated for this time-point – the range of SNRs that could be simulated was as large as possible for the 4.5-h time-point. This limited upper bound in SNR, biases the $\overline{SNR_w}$ (=25) to a value which is lower than would have been obtained if a broader range of SNR were available. A second set of images generated at a fixed time-point that spanned a greater range of SNRs, similar to the 1.8-h data, may have helped to verify that the major determinant for image quality is SNR. Nonetheless, we have shown that resolution is not the decisive parameter upon which imaging optimization should be based. Instead, optimal image quality occurs consistently for an SNR of 30–35. In

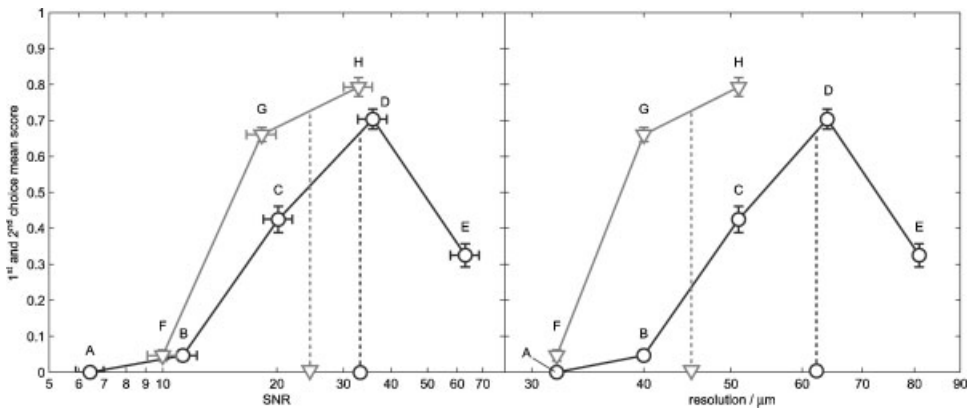

Figure 5. First and second choice mean score for experiment 1 (1.8-h data, ○) and higher quality images in experiment 5 (4.5-h data, ▽). Scores are plotted *versus* SNR (left) and resolution (right). The dashed lines represent the calculated weighted mean preferred SNRs ($\overline{SNR_w}$, left) and weighted mean preferred resolutions ($\overline{res_w}$, right) for each imaging time. Horizontal error bars are absent in the right panel as resolution values of the tradeoff images were predetermined.

Copyright © 2009 John Wiley & Sons, Ltd.

another study, we have shown that maximal information content in an image occurs at a fixed SNR and is independent of resolution (S. Portnoy, S. C. Kale, A. Feintuch, C. Tardiff, G. B. Pike, R. M. Henkelman. Information content of SNR/resolution tradeoffs in three dimensional MR Imaging. *Med. Phys.* 2008; submitted for publication).

DISCUSSION

In MR imaging, limited scan time means the operator must make a decision of how to balance SNR and resolution for optimal viewing of anatomy and pathology. In this study, participants were requested to identify images which best provided such anatomical information. All readers had adequate visual acuity to interpret the features in the presented images and make competent evaluations.

An early investigation of reader preference for SNR and resolution in MR images was presented by Owen and Wehrli (14) in 1990. In this study, readers used a five-point scale to rate the quality of T_1-weighted brain and knee images, which were acquired at variable scan times. The authors concluded that SNR in excess of 20 should be spent on improving the resolution. That conclusion clearly differs from the results found here. We found that images with a mean SNR of 20 were 40% less preferred than images with SNR ~36 in experiment 1. The choice of MR image contrast is unlikely to account for the difference: for example using T_1-weighted images *versus* T_2-weighted images. However, Owen and Wehrli did not fix the scan time and compared images of varying overall quality. This inevitably biases selection toward images produced at longer scan time. Further, the sequence design strategy is usually to acquire higher resolution data over increased signal averaging for longer scan times, and therefore preference is shifted to lower SNR images with greater resolution.

Rubenstein *et al*. (15) also considered SNR and resolution requirements in MR, but specifically for the accurate detection of morphologic changes in degenerative cartilage. One part of their study explored the detectability of pathology in cartilage when imaging time was fixed. From this study, they agreed with Owen and Wehrli that SNR should be traded for resolution until a value of ~20 is reached when variable gradient strengths are used. Note that this finding may be biased to high contrast details necessary to examine fraying and fragmentation in pathologic cartilage which would explain the shift of preference to images with better resolutions and lower SNRs as demonstrated in experiment 5. Additionally, in the Rubenstein paper, the change in SNR between the compared images was very large, jumping 4× from 19 to 76, perhaps overstepping a better suited image for reading with an intermediate SNR.

Alternatively, low contrast detectability as a function of resolution in MR has been evaluated by Constable and Henkelman (7) who took a similar approach to us by considering resolution and SNR at *fixed scan time* and bandwidth. Constable and Henkelman point out that rebinning a high-resolution image to a lower resolution image does not recover the SNR and contrast is lost when initially acquiring high-resolution data. This is not the case for imaging modalities using ionizing radiation. Furthermore, this study is likely the first to show both theoretically (through a simple formulation) and experimentally (by producing simulated contrast–detail curves) that the expected detectability of low-contrast signal does not change when rebinning. The author thus emphasizes that one needs to give consideration to the sacrifice of low contrast detectability when acquiring high-resolution data at fixed imaging time. Our study essentially extends this work by searching for and determining the optimum tradeoff between SNR (and therefore contrast) and resolution in anatomical images.

An interesting comparison can be made between the results obtained here for the optimal tradeoff for viewing to the optimal tradeoff for computer analysis in image registration. While it was found here that the human observer requires images with an SNR approximately between 30 and 35, it was found that our registration procedures appear to be optimized when the voxel SNR is approximately 20 (16). This suggests that the human observer is more willing to tradeoff fine details and structures in the image for greater SNR, whereas computer registration algorithms have a greater tolerance to noise and produce optimal results at finer resolutions.

In our simulation of the SNR–resolution tradeoff implementation, no restriction was imposed on the length of the readout time and we were able to ignore T_2 apodization as the readout time was much less than the T_2 of 28 ms. This situation, where resolution in the readout direction can be acquired without prolonging the total imaging time, is common in MR imaging but that is not always the case. Protocols that require fast imaging where TRs are very short and the system is reading out data nearly continuously, such as in spiral imaging or steady-state pulse sequences, impose limitations on the sampling time. In these cases increases in resolution can only be made through increases in gradient strength and thus bandwidth, which in turn changes the tradeoff between SNR and resolution. For example, when sampling time is limited, doubling the resolution in the readout direction decreases the SNR by an additional factor of $\sqrt{2}$ (compared to the fixed-bandwidth case) because the associated doubling of bandwidth increases the standard deviation of noise by $\sqrt{2}$.

It was determined that the optimal tradeoff for viewing is achieved when voxel sizes are chosen such that image SNR is approximately in the range of 30–35. This determination was made given a specific set of parameters including: a 7-T magnet, T_2-weighted image contrast, an FSE pulse sequence, mouse neuroanatomy, and a generic detectability task. However, this result should be generally applicable, independent of specific imaging systems and anatomy. If the image-specific parameters were changed, all emulated tradeoff images would be affected equally in terms of the change in contrast, SNR, and even artifacts. Consequently, the *relative* reader ratings would be expected to remain the same ensuring that SNR is still the major determinant of interpretability. Further, the use of mouse neuroanatomy does not restrict the generality of the conclusions. It is expected that these conclusions should be applicable to human imaging as well, because the mouse brain images contained a range of contrasts at varying spatial scales that can be said to fairly represent a general anatomical image. In fact, the power spectral density of MR images, i.e. the squared magnitude of *k*-space, has been shown to possess a $\|\mathbf{k}\|^{-\alpha}$ characteristic, with $\alpha \approx 3$, in both humans (9) and mice (17). This is a general observation among natural scene and fractal images: that $\|\mathbf{k}\|^{-\alpha}$ spatial statistics are scale-invariant (18). Although not a conclusive proof, the implication of this similarity is that evaluation of human and mouse anatomical MR images are comparable.

This is not to imply that optimizing MR pulse sequences is simply a matter of ensuring an ideal SNR. Instead, the most important issue in clinical imaging is ensuring appropriate

Copyright © 2009 John Wiley & Sons, Ltd.

contrast (using pulse sequences and contrast agents) of the pathology to be detected. However, once the contrast decision is made, the SNR-resolution tradeoff still remains and an answer is provided in this paper.

In conclusion, we have demonstrated that for chosen contrast and a fixed scan time in MR imaging, the optimal viewing of anatomical images was found to be at an SNR in the range of ~30–35. It is recommended that image resolution be chosen to produce this target voxel SNR. There are two expected exceptions to this imaging guideline when *a priori* information about the feature(s)-of-interest are known. The first is when the minimum SNR requirements to discern subtle tissue contrasts between specific tissues are greater than the prescribed SNR range. The other situation is when the scale of the feature of interest is below the resulting imaging resolution when SNR is 30–35. These cases are essentially the reading tasks of experiments 3 and 4 – the results of which suggested images with more SNR and more resolution, respectively.

Acknowledgements

This work is a part of the Mouse Imaging Centre (MICe) at the Hospital for Sick Children and the University of Toronto. The authors would like to thank Victoria Bonn, Jun Dazai, Jonathan Bishop, and Brian Nieman for specimen preparation and development of the imaging protocols. Dr R. Mark Henkelman holds a Canada Research Chair in Imaging; Shoan Kale is a recipient of a NSERC graduate scholarship.

REFERENCES

1. Parker DL, Gullberg GT. Signal-to-noise efficiency in magnetic resonance imaging. Med. Phys. 1990; 17: 250–257.
2. Redpath TW. Signal-to-noise ratio in MRI. Br. J. Radiol. 1998; 71: 704–707.
3. Nishimura D. Noise considerations. In Nishimura D (ed.). *Principles of Magnetic Resonance Imaging*. Stanford University Press: Palo Alto, CA, 1996; p 158–168.
4. Pruessmann KP, Weiger M, Scheidegger MB, Boesiger P. SENSE: sensitivity encoding for fast MRI. Magn. Reson. Med. 1999; 42: 952–962.
5. Nieman BJ, Bock NA, Bishop J, Sled JG, Chen XJ, Henkelman RM. Fast spin-echo for multiple mouse magnetic resonance phenotyping. Magn. Reson. Med. 2005; 54: 532–537.
6. Black RD, Early TA, Roemer PB, *et al*. A high-temperature superconducting receiver for nuclear magnetic resonance microscopy. Science 1993; 259: 793.
7. Constable RT, Henkelman RM. Contrast, resolution, and detectability in MR imaging. J. Comput. Assist. Tomogr. 1991; 15: 297–303.
8. Edelstein WA, Glover GH, Hardy CJ, Redington RW. The intrinsic signal-to-noise ratio in NMR imaging. Magn. Reson. Med. 1986; 3: 604–618.
9. Fuderer M. The information content of MR images. IEEE Trans. Med. Imaging 1988; 7: 368–380.
10. Henkelman RM, Dazai J, Lifshitz N, *et al*. High throughput microimaging of the mouse brain. Proc. Int. Soc. Mag. Reson. Med. 2006; 2010, 14: 396.
11. Tyszka JM, Readhead C, Bearer EL, Pautler RG, Jacobs RE. Statistical diffusion tensor histology reveals regional dysmyelination effects in the shiverer mouse mutant. Neuroimage 2006; 29: 1058–1065.
12. Henkelman RM. Measurement of signal intensities in the presence of noise in MR images. Med. Phys. 1985; 12: 232–233.
13. Anonymous. Descriptive statistics. In: Zwillinger D (ed.). *CRC Standard Mathematical Tables and Formulae*, 30th edn. CRC Press: Boca Raton, FL, 1996; p 601–603.
14. Owen RS, Wehrli FW. Predictability of SNR and reader preference in clinical MR imaging. Magn. Reson. Imaging 1990; 8: 737–745.
15. Rubenstein JD, Li JG, Majumdar S, Henkelman RM. Image resolution and signal-to-noise ratio requirements for MR imaging of degenerative cartilage. Am. J. Roentgenol. 1997; 169: 1089–1096.
16. Kale SC, Lerch JP, Henkelman RM, Chen XJ. Optimization of the SNR-resolution tradeoff for registration in magnetic resonance images. Hum. Brain Mapp. 2008. 29: 1147–1158.
17. Behin R, Bishop J, Henkelman RM. Dynamic range requirements for MRI. Concepts Magn. Reson. 2005; 26B: 28–35.
18. Field DJ. Relations between the statistics of natural images and the response properties of cortical cells. J. Opt. Soc. Am. A 1987; 4: 2379–2394.

Copyright © 2009 John Wiley & Sons, Ltd.